

Chiral symmetry breaking with lattice propagators

A. C. Aguilar^{1,*} and J. Papavassiliou^{2,†}

¹*Federal University of ABC, CCNH,*

Rua Santa Adélia 166, CEP 09210-170, Santo André, Brazil.

²*Department of Theoretical Physics and IFIC,*

University of Valencia-CSIC, E-46100, Valencia, Spain.

Abstract

We study chiral symmetry breaking using the standard gap equation, supplemented with the infrared-finite gluon propagator and ghost dressing function obtained from large-volume lattice simulations. One of the most important ingredients of this analysis is the non-abelian quark-gluon vertex, which controls the way the ghost sector enters into the gap equation. Specifically, this vertex introduces a numerically crucial dependence on the ghost dressing function and the quark-ghost scattering amplitude. This latter quantity satisfies its own, previously unexplored, dynamical equation, which may be decomposed into individual integral equations for its various form factors. In particular, the scalar form factor is obtained from an approximate version of the “one-loop dressed” integral equation, and its numerical impact turns out to be rather considerable. The detailed numerical analysis of the resulting gap equation reveals that the constituent quark mass obtained is about 300 MeV, while fermions in the adjoint representation acquire a mass in the range of (750-962) MeV.

PACS numbers: 12.38.Lg, 12.38.Aw, 12.38.Gc

*Electronic address: Arlene.Aguilar@ufabc.edu.br

†Electronic address: Joannis.Papavassiliou@uv.es

I. INTRODUCTION

The dynamical mechanism responsible for chiral symmetry breaking (CSB) in QCD has been the focal point of extensive research during several years [1–15]. The study of CSB in the continuum involves almost invariably some version of the Schwinger-Dyson equation (SDE) for the quark propagator (gap equation). This non-linear integral equation has a notoriously rich structure, being extremely sensitive to the details of its kernel; the latter is composed by the various non-perturbative ingredients entering into the gap equation, most notably the gluon propagator and the quark gluon vertex. As is well-known, the gap equation displays “critical” behavior: the support of the kernel throughout the entire range of integration must exceed a certain critical value in order to generate non-trivial solutions for the quark propagator [3]. Given that most of this support originates from the infrared region, i.e. around the QCD mass scale of a few hundred MeV, the study of CSB through the gap equation furnishes stringent probes on the various methods and models aiming towards a quantitative description of the non-perturbative sector of QCD.

In recent years, a large number of independent large-volume lattice simulations have furnished highly non-trivial information on the infrared (IR) behavior of two fundamental ingredients of pure Yang-Mills theories, namely the (quenched) gluon and ghost propagators, for both $SU(2)$ and $SU(3)$ [16–21]. In particular, these simulations have firmly established that (in the Landau gauge) the QCD gluon propagator and the ghost dressing function are IR finite and non-vanishing [22–24].

Given that the lattice is expected to capture reliably the full non-perturbative information contained in the gluon and ghost propagators, it is natural to explore their consequences for CSB. To that end, in this article we use lattice results for these Green’s functions as inputs for the gap equation, and study the emerging CSB pattern for quarks (fundamental representation) and for fermions in the adjoint representation. Specifically, we will employ the lattice data of [18], given that they perform $SU(3)$ simulations for both the gluon and the ghost propagators. As it will become clear from the results presented in the main body of the paper, the analysis carried out here may be regarded as a serious test of the robustness of the aforementioned lattice results, and can serve as a characteristic example of the rich phenomenology that one may extract with them.

The detailed implementation of the idea described above is far from straightforward,

mainly due to the complicated structure of the gap equation, which makes it difficult to determine its exact dependence on the aforementioned lattice ingredients (propagators). In fact, of particular importance for the self-consistency of the whole picture is the role played by the ghost sector (see, e.g. [11], and references therein). The way the ghost sector enters into the gap equation is through the fully-dressed quark-gluon vertex. Specifically, recall that, in virtually all treatments, the fully-dressed quark-gluon vertex is not obtained from the corresponding dynamical equation (the SDE of the vertex), but is rather expressed in terms of the quark propagator, such that its Slavnov-Taylor identity (STI) is automatically satisfied (this procedure is known as the “gauge technique” [25]). The STI itself contains explicit reference to both the ghost dressing function and the so-called “quark-ghost scattering kernel” [26]; the latter is given by its own dynamical equation, and, as we will see, its numerical impact to the solutions obtained from the gap equation is quite important. If, instead, one were to “abelianize” this part of the problem by assuming that the quark-gluon vertex satisfies a QED-like Ward identity rather than the correct (non-abelian) STI, the resulting gap equation would contain the gluon propagator as its sole ingredient, a fact that would lead to an apparent incompatibility, in the sense that the kernel would not exceed the critical value (no CSB), or would fail to generate realistic constituent quark masses [6, 7, 10, 15].

The main results of the present article may be summarized as follows:

(a) The non-abelian Ansatz for the full quark-gluon vertex depends explicitly on the ghost-dressing function and the quark-ghost scattering kernel; the latter quantity has a rather complicated Dirac structure [27], being composed by four independent form factors [see Eq. (2.10)]. As a consequence, the corresponding expressions for the form factors appearing in the Lorentz decomposition for the longitudinal part of the quark-gluon vertex [see Eq. (3.1)] are modified (with respect to the case where the quark-ghost scattering kernel is set to its tree-level value); their full form is presented in Eq. (3.5). As a result, the gap equation acquires a more complicated structure, given in Eqs. (3.11)-(3.12). To the best of our knowledge, both Eq. (3.5) and Eqs. (3.11)-(3.12) appear for the first time in the literature.

(b) The quark-ghost scattering kernel satisfies its own dynamical equation, which may be decomposed into individual integral equations for the various form factors entering into the gap equation. In turn, these integral equations depend, among other quantities, on the quark propagator, a fact which converts the full treatment of the problem into the solution

of a complicated system of various coupled integral equations.

(c) In order to make the above system of equations more tractable, without compromising its main features, we retain only the dependence of the gap equation on the scalar form factor of the quark-ghost scattering kernel, discarding all other form factors. In addition, we choose a very particular kinematic configuration, which further simplifies the corresponding integral equation that determines the aforementioned quantity. The final “one-loop dressed” equation is given in Eq. (3.16), and constitutes, to the best of our knowledge, a novel result. For the actual calculation of the scalar form factor we will use on the rhs of Eq. (3.16) the lattice results of [18], and then substitute the result (shown in Fig. 6) into the gap equation.

(d) A well-known endemic shortcoming of all approaches based on the gauge-technique is that the transverse (i.e. identically conserved) part of the (quark-gluon) vertex remains largely undetermined; this fact, in turn, distorts the cancellations of overlapping divergences, the multiplicative renormalizability of the Green’s functions in question, and their compliance with the renormalization group (RG). The construction of the appropriate transverse piece has been carried out in detail for the case of QED [28], but no real progress has been made in a non-abelian context. As is common practice, the aforementioned problem is remedied by multiplying (by hand) the kernel of the gap equation by an appropriate functions, which restores the desired properties. For the case at hand, the simplest quantity that accounts for the missing dynamics is the full ghost dressing-function. As we will explain in the corresponding subsection, this choice is dictated by the STI satisfied by the quark-gluon vertex, and enforces the correct RG behavior of the dynamical (running) mass obtained from the gap equation. It should be stressed that the inclusion of the dressing-function has a considerable numerical impact on the obtained CSB solution, boosting up the quark mass to phenomenologically acceptable values.

(e) After substituting all necessary ingredients comprising its kernel, the resulting gap equation is finally solved numerically, for two different cases. First, we study fermions in the fundamental representation (quarks), obtaining a quark mass that in the IR is about 300 MeV. Second, we consider CSB with fermions in the adjoint representation; the latter are particularly interesting, due to the clear separation between chiral symmetry restoration and deconfinement they display [29–31]. The corresponding mass obtained for the adjoint fermions is within the range (750-962) MeV, depending on the details of the quark-gluon vertex used. This values are not too far from what one would expect naively, given the

enhancement of $9/4$ produced to the kernel of the adjoint gap equation due to the ratio of the Casimir eigenvalues of the two representations.

The article is organized as follows. In Section II we introduce the necessary notation, and review the general the structure of the gap equation. In Section III we first construct an Ansatz for the quark-gluon vertex which makes full reference on the quark-ghost scattering kernel, and use this vertex to derive the corresponding gap equation. Then, the “one-loop dressed” approximation for the scalar part of the quark-ghost scattering kernel is set up, and the improvements necessary for restoring the correct RG properties are discussed in detail. In Section IV we present the main results of this work. In particular, after briefly reviewing the recent lattice results on the gluon and ghost propagators that enter into the gap equation, we proceed to the numerical solution of the gap equation. In Section V we discuss our results and comment on possible future directions. Finally, in an Appendix we analyze for completeness the structure of the gap equation within the framework of the pinch technique (PT) [32–34] or, equivalently, the background field method (BFM) [35].

II. GENERAL STRUCTURE OF THE GAP EQUATION

In this section we will introduce the basic definitions and ingredients necessary for the study of the quark SDE (gap equation). Then, we will give a special emphasis in the construction of a general Ansatz for full fermion-gluon vertex, where its non-abelian character will be kept intact. Finally, we will incorporate it into the gap equation and explore its effects.

A. Definitions and ingredients

Let us first introduce the necessary notation. In covariant gauges, the inverse of the full quark propagator in the Minkowski space has the general form [26]

$$S^{-1}(p) = \not{p} - m - \Sigma(p), \quad (2.1)$$

where m is the bare current quark mass, and $\Sigma(p)$ the quark self-energy. It is common practice to decompose $\Sigma(p)$, in terms of a Dirac vector component, $A(p^2)$, and a scalar component, $B(p^2)$, which allow us to define the dynamical quark mass function as being the

ratio $\mathcal{M}(p^2) = B(p^2)/A(p^2)$, explicitly we have [9]

$$S^{-1}(p) = A(p^2)\not{p} - B(p^2)\mathbb{I} = A(p^2)[\not{p} - \mathcal{M}(p^2)\mathbb{I}], \quad (2.2)$$

where \mathbb{I} is the identity matrix, and the term $A^{-1}(p^2)$ is often referred to in the literature as the “fermion wave function”. Note that, the fermion acquires a dynamical mass as long as $B(p^2)$ is different from zero. Therefore, the CSB will be signaled when we obtain $B(p^2) \neq 0$.

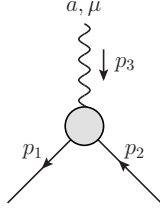


FIG. 1: The full fermion-gluon vertex.

In addition, the gluon propagator $\Delta_{\mu\nu}(q)$ in the covariant renormalizable (R_ξ) gauges, has the form

$$\Delta_{\mu\nu}(q) = -i \left[P_{\mu\nu}(q)\Delta(q^2) + \xi \frac{q_\mu q_\nu}{q^4} \right], \quad (2.3)$$

where ξ denotes the gauge-fixing parameter, and

$$P_{\mu\nu}(q) = g_{\mu\nu} - q_\mu q_\nu / q^2, \quad (2.4)$$

is the usual transverse projector. In this work, we are particularly interested in the Landau gauge which is reached when $\xi = 0$. Moreover, the full ghost propagator $D(q^2)$ and its dressing function $F(q^2)$ are related by

$$D(q^2) = \frac{iF(q^2)}{q^2}. \quad (2.5)$$

An essential ingredient in our study is the fermion-gluon vertex, represented in Fig. 1, and given by

$$\Gamma_\mu^a(p_1, p_2, p_3) = gT^a\Gamma_\mu(p_1, p_2, p_3), \quad (2.6)$$

with T^a ($a = 1, 2, \dots, N^2 - 1$) being the generators of the group $SU(N)$ where the fermions are assigned. The matrices T^a are hermitian and traceless, generating the closed algebra

$$[T^a, T^b] = if^{abc}T^c, \quad (2.7)$$

$$H(p_1, p_2, p_3) = \text{Diagram}$$

FIG. 2: Diagrammatic representation of the fermion-ghost scattering kernel $H(p_1, p_2, p_3)$.

where f^{abc} are the (totally antisymmetric) structure constants. In the case of $SU(3)$, and for fermions in the fundamental representations (quarks), we have that $T^a = \lambda^a/2$, where λ^a are the Gell-Mann matrices. When fermions are in the adjoint, $(T^a)^{bc} = -if^{abc}$.

The vertex $\Gamma_\mu(p_1, p_2, p_3)$ satisfies the fundamental STI [26]

$$p_3^\mu \Gamma_\mu(p_1, p_2, p_3) = F(p_3)[S^{-1}(-p_1)H(p_1, p_2, p_3) - \overline{H}(p_2, p_1, p_3)S^{-1}(p_2)], \quad (2.8)$$

where the fermion-ghost scattering kernel $H(p_1, p_2, p_3)$ is defined diagrammatically in Fig. 2, and is written as

$$H^a(p_1, p_2, p_3) = T^a H(p_1, p_2, p_3). \quad (2.9)$$

The kernel $H(p_1, p_2, p_3)$ and the “conjugated” $\overline{H}(p_2, p_1, p_3)$ have the following Lorentz decomposition [27] (note the change $p_1 \leftrightarrow p_2$ in the arguments of the latter)

$$\begin{aligned} H(p_1, p_2, p_3) &= X_0 \mathbb{I} + X_1 \not{p}_1 + X_2 \not{p}_2 + X_3 \tilde{\sigma}_{\mu\nu} p_1^\mu p_2^\nu, \\ \overline{H}(p_2, p_1, p_3) &= \overline{X}_0 \mathbb{I} - \overline{X}_2 \not{p}_1 - \overline{X}_1 \not{p}_2 + \overline{X}_3 \tilde{\sigma}_{\mu\nu} p_1^\mu p_2^\nu, \end{aligned} \quad (2.10)$$

where the form factors X_i are functions of the momenta, $X_i = X_i(p_1, p_2, p_3)$, and we use the notation $\overline{X}_i(p, r, q) \equiv X_i(r, p, q)$ and $\tilde{\sigma}_{\mu\nu} \equiv \frac{1}{2}[\gamma_\mu, \gamma_\nu]$ (Note the difference between $\tilde{\sigma}_{\mu\nu}$ and the usually defined $\sigma_{\mu\nu} = \frac{i}{2}[\gamma_\mu, \gamma_\nu]$).

B. The renormalized gap equation

The SDE for the fermion propagator is diagrammatically represented in Fig. 3. Using the momenta flow and Lorentz indices indicated in Fig. 3, the gap equation can be written as

$$S^{-1}(p) = \not{p} - m - C_r g^2 \int_k \Gamma_\mu^{[0]} S(k) \Gamma_\nu(-p, k, q) \Delta^{\mu\nu}(q), \quad (2.11)$$

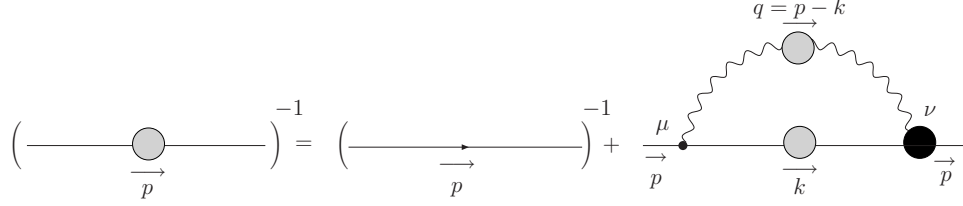


FIG. 3: The SDE for the fermion propagator given by Eq. (2.11). The gray blobs represent the fully dressed gluon and quark propagators, while the black blob denotes the dressed fermion-gluon vertex.

where $q \equiv p - k$, $\int_k \equiv \mu^{2\epsilon}(2\pi)^{-d} \int d^d k$, with $d = 4 - \epsilon$ the dimension of space-time, and $\Gamma_\mu^{[0]}$ is the fermion-gluon vertex at tree level. C_r is the Casimir eigenvalue of the given fermion representation ($r = F$ for the fundamental, and $r = A$ for the adjoint). More specifically, for the gauge group $SU(3)$, we have $C_A = 3$ and $C_F = 4/3$. Note that, m is a current fermion mass, the same appearing in the QCD Lagrangian, and in case of $m \neq 0$ in Eq. (2.11), the chiral symmetry is explicitly broken. In this work, we will consider the case $m = 0$, i.e., the chiral symmetry is kept intact at the Lagrangian level.

All quantities appearing in Eq. (2.11) are unrenormalized; they are related to their respective renormalized counterparts, denoted with a subscript “R”, through the relations [36]

$$\begin{aligned}
S_R(p; \mu) &= Z_F^{-1}(\mu)S(p), \\
\Delta_R(q; \mu) &= Z_A^{-1}(\mu)\Delta(q), \\
F_R(q; \mu) &= Z_c^{-1}(\mu)F(q), \\
\Gamma_R^\nu(p, k, q; \mu) &= Z_1(\mu)\Gamma^\nu(p, k, q), \\
g_R(\mu) &= Z_g^{-1}(\mu)g = Z_1^{-1}Z_F^1Z_A^{1/2}g,
\end{aligned} \tag{2.12}$$

where Z_F , Z_A , Z_c , Z_1 , and Z_g are the corresponding renormalization constants. Substituting Eqs. (2.12) into Eq. (2.11), we obtain

$$S_R^{-1}(p) = Z_F \not{p} - Z_1 C_r g_R^2 \int_k \gamma_\mu S_R(k) \Gamma_{R\nu}(-p, k, q) \Delta_R^{\mu\nu}(q). \tag{2.13}$$

In addition, the STIs of Eq. (2.8) imposes the all-order constraint

$$Z_1 = Z_c^{-1} Z_F Z_H^{-1}, \tag{2.14}$$

where Z_H is the renormalization constant needed for the quark-ghost kernel, i.e., $H = Z_H^{-1} H_R$. Now, in the Landau gauge, both the quark self-energy and the quark-ghost

kernel are finite at one-loop; thus, at that order, $Z_F = Z_H = 1$, and, therefore, $Z_1 = Z_c^{-1}$, i.e., at one-loop the quark-gluon vertex renormalizes as the inverse the ghost propagator. Imposing the above approximation in the Eq. (2.13), we obtain

$$S^{-1}(p) = \not{p} - Z_c^{-1} C_r g^2 \int_k \gamma_\mu S(k) \Gamma_\nu(-p, k, q) \Delta^{\mu\nu}(q), \quad (2.15)$$

where we have suppressed the subscript ‘‘R’’ to avoid notation clutter.

III. INFLUENCE OF THE GHOST SECTOR ON THE GAP EQUATION

In this rather lengthy and technical section we study in detail how the ghost sector enters into the gap equation. To that end, in subsection III A we will use the STI to determine the dependence of the form factors of the longitudinal part of the quark-gluon vertex on the corresponding form factors X_i appearing in the Dirac decomposition of the quark-ghost scattering kernel, given in Eq. (2.10). Then, we will use the resulting vertex in order to derive the most general expression for the gap equation, displaying the dependence on all form factors X_i . In subsection III B we derive the ‘‘one-loop dressed’’ expression for the scalar form factor X_0 , which is the only one that will be considered in the ensuing analysis. The modifications introduced into some standard forms of the quark-gluon vertex vertex, and the form of the gap equations obtained with them are presented in subsection III C. Finally, the adjustments necessary in order to enforce the correct RG properties of the gap equation are discussed in subsection III D.

A. The full fermion-gluon vertex

The most general Lorentz decomposition for the longitudinal part of the vertex $\Gamma_\mu(p_1, p_2, p_3)$ can be written as [27]

$$\Gamma_\mu(p_1, p_2, p_3) = L_1 \gamma_\mu + L_2 (\not{p}_1 - \not{p}_2)(p_1 - p_2)_\mu + L_3 (p_1 - p_2)_\mu + L_4 \tilde{\sigma}_{\mu\nu} (p_1 - p_2)^\nu, \quad (3.1)$$

where L_i are the form factors, whose dependence on the momenta has been suppressed, in order to keep a compact notation *i.e.* $L_i = L_i(p_1, p_2, p_3)$. The tree level expression is recovered setting $L_1 = 1$ and $L_2 = L_3 = L_4 = 0$; then, $\Gamma_\mu^{[0]}(p_1, p_2, p_3) = \gamma_\mu$.

Due to the fact that the behavior of the vertex $\Gamma_\mu(p_1, p_2, p_3)$ is constrained by the STI of Eq. (2.8), the form factors L_i 's appearing into the Eq. (3.1) will be given in terms of the form factors X_i 's of Eq. (2.10).

More specifically, using the standard decomposition of $S^{-1}(p)$ expressed in Eq. (2.2), it is relatively straightforward to demonstrate that the rhs of Eq. (2.8) becomes

$$p_3^\mu \Gamma_\mu(p_1, p_2, p_3) = F(p_3)[C_0 \mathbb{I} + C_1 \not{p}_1 + C_2 \not{p}_2 + C_3 \tilde{\sigma}_{\mu\nu} p_1^\mu p_2^\nu], \quad (3.2)$$

with

$$\begin{aligned} C_0 &= -A(p_1) (p_1^2 X_1 + p_1 \cdot p_2 X_2) + A(p_2) (p_2^2 \bar{X}_1 + p_1 \cdot p_2 \bar{X}_2) - B(p_1) X_0 - B(p_2) \bar{X}_0; \\ C_1 &= A(p_1) (p_1 \cdot p_2 X_3 - X_0) - p_2^2 A(p_2) \bar{X}_3 - B(p_1) X_1 + B(p_2) \bar{X}_2; \\ C_2 &= A(p_2) (p_1 \cdot p_2 \bar{X}_3 - \bar{X}_0) - p_1^2 A(p_1) X_3 - B(p_1) X_2 - B(p_2) \bar{X}_1; \\ C_3 &= A(p_2) \bar{X}_2 - A(p_1) X_2 - B(p_1) X_3 + B(p_2) \bar{X}_3. \end{aligned} \quad (3.3)$$

On the other hand, contracting Eq. (3.1) with p_3^μ , we have

$$p_3^\mu \Gamma_\mu(p_1, p_2, p_3) = (p_2^2 - p_1^2) L_3 \mathbb{I} + [(p_2^2 - p_1^2) L_2 - L_1] \not{p}_1 - [(p_2^2 - p_1^2) L_2 + L_1] \not{p}_2 - 2L_4 \tilde{\sigma}_{\mu\nu} p_1^\mu p_2^\nu. \quad (3.4)$$

Equating the right-hand sides of Eq. (3.2) and Eq. (3.4), we can express the L_i 's in terms of the functions A , B and X_i 's. Specifically,

$$\begin{aligned} L_1 &= \frac{F(p_3)}{2} \left\{ A(p_1)[X_0 + (p_1^2 - p_1 \cdot p_2) X_3] + A(p_2)[\bar{X}_0 + (p_2^2 - p_1 \cdot p_2) \bar{X}_3] \right\} \\ &\quad + \frac{F(p_3)}{2} \left\{ B(p_1)(X_1 + X_2) + B(p_2)(\bar{X}_1 + \bar{X}_2) \right\}; \\ L_2 &= \frac{F(p_3)}{2(p_2^2 - p_1^2)} \left\{ A(p_1)[(p_1^2 + p_1 \cdot p_2) X_3 - X_0] - A(p_2)[(p_2^2 + p_1 \cdot p_2) \bar{X}_3 - \bar{X}_0] \right\} \\ &\quad + \frac{F(p_3)}{2(p_2^2 - p_1^2)} \left\{ B(p_1)(X_2 - X_1) + B(p_2)(\bar{X}_1 - \bar{X}_2) \right\}; \\ L_3 &= -\frac{F(p_3)}{p_2^2 - p_1^2} \left\{ A(p_1) (p_1^2 X_1 + p_1 \cdot p_2 X_2) - A(p_2) (p_2^2 \bar{X}_1 + p_1 \cdot p_2 \bar{X}_2) + B(p_1) X_0 - B(p_2) \bar{X}_0 \right\}; \\ L_4 &= \frac{F(p_3)}{2} \left\{ A(p_1) X_2 - A(p_2) \bar{X}_2 + B(p_1) X_3 - B(p_2) \bar{X}_3 \right\}. \end{aligned} \quad (3.5)$$

The standard approximation in the literature is to use the tree-level value of $H(p_1, p_2, p_3)$, which is equivalent to setting $X_0 = \bar{X}_0 = 1$ and $X_i = \bar{X}_i = 0$, for $i \leq 1$, in the above equation. In addition, the effects of the ghost-dressing are also neglected, by imposing

$F(p_3) = 1$. In this limit, we obtain the following expressions

$$\begin{aligned}
L_1 &= \frac{A(p_1) + A(p_2)}{2}; \\
L_2 &= \frac{A(p_1) - A(p_2)}{2(p_1^2 - p_2^2)}; \\
L_3 &= \frac{B(p_1) - B(p_2)}{p_1^2 - p_2^2}; \\
L_4 &= 0;
\end{aligned} \tag{3.6}$$

which leads to the so-called Ball-Chiu (BC) vertex [38]

$$\begin{aligned}
\Gamma_{\text{BC}}^\mu(p_1, p_2, p_3) &= \frac{A(p_1) + A(p_2)}{2} \gamma^\mu \\
&+ \frac{(p_1 - p_2)^\mu}{p_1^2 - p_2^2} \left\{ [A(p_1) - A(p_2)] \frac{\not{p}_1 - \not{p}_2}{2} + [B(p_1) - B(p_2)] \right\}.
\end{aligned} \tag{3.7}$$

We will next insert into Eq. (2.15) the general quark-gluon vertex of Eq. (3.1) with the expressions for the form factors L_i given in Eq. (3.5). Defining $p_1 = -p$, $p_2 = k$, and $p_3 = q$ and taking appropriate traces, it is straightforward to derive the following expressions for the integral equations satisfied by $A(p^2)$ and $B(p^2)$

$$\begin{aligned}
p^2 A(p^2) &= p^2 - Z_c^{-1} C_r g^2 \left\{ \int_k \frac{L_1(2p_\mu p_\nu - k \cdot p g_{\mu\nu}) + 2(k^2 + p^2)L_2 p_\mu p_\nu}{A^2(k^2)k^2 - B^2(k^2)} \Delta^{\mu\nu}(q) A(k^2) \right. \\
&+ \left. \int_k \frac{p \cdot (k + p)L_4 g_{\mu\nu} - 2(L_3 + L_4)p_\mu p_\nu}{A^2(k^2)k^2 - B^2(k^2)} \Delta^{\mu\nu}(q) B(k^2) \right\},
\end{aligned} \tag{3.8}$$

$$\begin{aligned}
B(p^2) &= Z_c^{-1} C_r g^2 \left\{ \int_k \frac{2(L_4 - L_3)p_\mu p_\nu - k \cdot (k + p)L_4 g_{\mu\nu}}{A^2(k^2)k^2 - B^2(k^2)} \Delta^{\mu\nu}(q) A(k^2) \right. \\
&+ \left. \int_k \frac{L_1 g_{\mu\nu} + 4L_2 p_\mu p_\nu}{A^2(k^2)k^2 - B^2(k^2)} \Delta^{\mu\nu}(q) B(k^2) \right\}.
\end{aligned} \tag{3.9}$$

Using that, for the gluon propagator in the Landau gauge, $\Delta_\mu^\mu(q) = -i3\Delta(q)$, and $p_\mu p_\nu \Delta^{\mu\nu}(q) = -ih(p, k)\Delta(q)$, where

$$h(p, k) \equiv \frac{[k^2 p^2 - (k \cdot p)^2]}{q^2}, \tag{3.10}$$

we can cast the gap equation in the form

$$\begin{aligned}
p^2 A(p) &= p^2 + iZ_c^{-1} C_r g^2 \left\{ \int_k \frac{2[(L_1 + (k^2 + p^2)L_2]h(p, k) - 3(k \cdot p)L_1}{A^2(k^2)k^2 - B^2(k^2)} \Delta(q) A(k^2) \right. \\
&+ \left. \int_k \frac{3p \cdot (k + p)L_4 - 2(L_3 + L_4)h(p, k)}{A^2(k^2)k^2 - B^2(k^2)} \Delta(q) B(k^2) \right\},
\end{aligned} \tag{3.11}$$

$$\begin{aligned}
B(p) = & -iZ_c^{-1}C_r g^2 \left\{ \int_k \frac{2(L_4 - L_3)h(p, k) - 3k \cdot (k + p)L_4}{A^2(k^2)k^2 - B^2(k^2)} \Delta(q)A(k^2) \right. \\
& \left. + \int_k \frac{3L_1 + 4h(p, k)L_2}{A^2(k^2)k^2 - B^2(k^2)} \Delta(q)B(k^2) \right\}. \tag{3.12}
\end{aligned}$$

B. The “one-loop dressed” approximation for X_0

In order to evaluate Eqs. (3.11) and (3.12) further, it is necessary to determine the behavior of the form factors X_i entering into the definition of the L_i through the Eq. (3.5).

From Eq. (2.10), one can project out the form factors X_i in the following way

$$\begin{aligned}
X_0 &= \frac{\text{Tr}\{H\}}{4}; \\
X_1 &= \frac{p_2^2 \text{Tr}\{\not{p}_1 H\} - (p_1 \cdot p_2) \text{Tr}\{\not{p}_2 H\}}{4[p_1^2 p_2^2 - (p_1 \cdot p_2)^2]}; \\
X_2 &= \frac{p_1^2 \text{Tr}\{\not{p}_2 H\} - (p_1 \cdot p_2) \text{Tr}\{\not{p}_1 H\}}{4[p_1^2 p_2^2 - (p_1 \cdot p_2)^2]}; \\
X_3 &= \frac{\text{Tr}\{\tilde{\sigma}_{\alpha\rho} p_1^\alpha p_2^\rho H\}}{4[(p_1 \cdot p_2)^2 - p_1^2 p_2^2]}. \tag{3.13}
\end{aligned}$$

It is clear from the diagrammatic representation given in Fig. 2 that $H(p_1, p_2, p_3)$, and its form factors given in Eq. (3.13), depend among other things, on the fully dressed quark propagator. Therefore, the treatment of the full gap equation given in Eqs. (3.11) and (3.12) boils down to a complicated system of several coupled integral equations. In order to make the problem at hand technically more tractable, we will only retain one of the form factors given in Eq. (3.13), and study it in an approximate kinematic configuration, which simplifies the resulting structures considerably. Specifically, we will only consider the form factor X_0 , and assume that $p_1 = p_2 \equiv p$, and $p = -p_3/2$, so that $X_0 = \overline{X}_0$.

Note that the momentum p_3 coincides with the momentum of the gluon in the gap equation; therefore we will denote $p_3 = q$, and $p = -q/2$. To obtain a non-perturbative estimate for X_0 , we will study the “one-loop dressed” contribution given by the diagram of Fig. 4.

Denoting the full gluon-ghost vertex by $G_\mu^{ab} = \delta^{ab}G_\mu$, the expression for $X_0^{[1]}$ reads

$$X_0^{[1]}(p, p, q) = 1 - i \left(\frac{1}{4} \right) \frac{C_A g^2}{2} \int_k \Delta^{\mu\nu}(k) D(k-p) G_\nu \text{Tr}\{S(k+q)\Gamma_\mu\}. \tag{3.14}$$

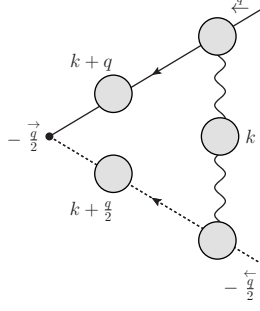


FIG. 4: Diagrammatic representation of the quark-ghost scattering kernel, $H(-q/2, -q/2, q)$, at one-loop.

To evaluate this further, we will use the following approximations: (i) G_ν will be replaced by its tree-level value, $G_\nu = (k-p)_\nu$. Note that, since the full $\Delta^{\mu\nu}(k)$ is transverse (Landau gauge), only the p_μ part survives. (ii) For the vertex Γ_μ we will use a slightly modified Ansatz than that of Eq. (3.7) [3, 12, 39], in order to reduce the algebraic complexity of the resulting equation.

Specifically, we will use as our starting point the Ansatz

$$\Gamma_\mu(q, -k-q, k) = \frac{1}{2} \left([A(k+q) + A(q)]\gamma_\mu + \frac{k_\mu}{k^2} [A(k+q) - A(q)](2\not{q} + \not{k}) \right), \quad (3.15)$$

which satisfies the STI of Eq. (2.8) in the chiral limit, $B = 0$, and with the ghost sector switched off ($F = H = 1$). Since the second term on the rhs of Eq. (3.15) is proportional to k_μ , it vanishes when inserted into (3.14), again due to the transversality of $\Delta^{\mu\nu}(k)$, a fact that simplifies considerably the resulting expressions.

According to the procedure discussed in the next section [see Eq. (3.22)], we will improve the Ansatz of Eq. (3.15) by multiplying it by $F(k)$, but keeping $H = 1$. Under these approximations, and after setting $p = -q/2$, Eq. (3.14) becomes (in Euclidean space)

$$X_0^{[1]}(q) = 1 + \frac{C_A g^2}{8} \int_k \left[q^2 - \frac{(q \cdot k)^2}{k^2} \right] \Delta(k) D\left(k + \frac{q}{2}\right) F(k) \frac{A(k+q)[A(k+q) + A(q)]}{A^2(k+q)(k+q)^2 + B^2(k+q)}. \quad (3.16)$$

We will finally approximate $A(k+q) = A(q) = 1$, and $B(k+q) = 0$, then we obtain

$$X_0^{[1]}(q) = 1 + \frac{1}{4} C_A g^2 q^2 \int_k [1 - f(k, q)] \Delta(k) F(k) \frac{F(k+q)}{(k+q)^4}, \quad (3.17)$$

where

$$f(k, q) \equiv \frac{(k \cdot q)^2}{k^2 q^2}. \quad (3.18)$$

After carrying out the integral on the rhs of Eq.(3.17) one obtains an approximate expression for $X_0^{[1]}(q)$ in terms of $\Delta(k)$ and $F(k)$; the result will be reported in section IV. Note that if we had multiplied Eq. (3.15) not only by $F(q)$ but also by $X_0^{[1]}(q)$, as is done in Eq. (3.22), then, instead of simply computing the integral of Eq. (3.17), one would have to deal with the more difficult task of solving an integral equation for the unknown $X_0^{[1]}(q)$.

C. The gap equation with ghost-improved quark-gluon vertices

There are two basic forms of the ‘‘abelianized’’ quark-gluon vertex usually employed in the literature: (i) the BC vertex, denoted by Γ_{BC}^μ , whose closed form is given in Eq. (3.7), and (ii) the so-called Curtis and Pennington (CP) vertex [40], to be denoted by Γ_{CP}^μ . These two vertices differ by a transverse (automatically conserved term), namely

$$\Gamma_{\text{CP}}^\mu(p_1, p_2, p_3) = \Gamma_{\text{BC}}^\mu(p_1, p_2, p_3) + \Gamma_{\text{T}}^\mu(p_1, p_2, p_3), \quad (3.19)$$

with

$$\Gamma_{\text{T}}^\mu(p_1, p_2, p_3) = \frac{\gamma^\mu(p_2^2 - p_1^2) - (p_1 - p_2)^\mu(\not{p}_1 + \not{p}_2)}{2d(p_1, p_2)} [A(p_2) - A(p_1)], \quad (3.20)$$

where

$$d(p_1, p_2) = \frac{1}{p_1^2 + p_2^2} \left\{ (p_2^2 - p_1^2)^2 + \left[\frac{B^2(p_2)}{A^2(p_2)} + \frac{B^2(p_1)}{A^2(p_1)} \right]^2 \right\}. \quad (3.21)$$

Evidently, under the approximations employed, the ghost effects due to $F(p_3)$ and $X_0^{[1]}(p_3)$ may be incorporated into these two vertices through simple multiplication of their form factors by $F(p_3)X_0^{[1]}(p_3)$. Denoting their ‘‘ghost-improved’’ versions by $\bar{\Gamma}_{\text{CP}}^\mu(p_1, p_2, p_3)$ and $\bar{\Gamma}_{\text{BC}}^\mu(p_1, p_2, p_3)$, respectively, we have

$$\begin{aligned} \bar{\Gamma}_{\text{BC}}^\mu(p_1, p_2, p_3) &= F(p_3)X_0^{[1]}(p_3)\Gamma_{\text{BC}}^\mu(p_1, p_2, p_3), \\ \bar{\Gamma}_{\text{CP}}^\mu(p_1, p_2, p_3) &= F(p_3)X_0^{[1]}(p_3)\Gamma_{\text{CP}}^\mu(p_1, p_2, p_3). \end{aligned} \quad (3.22)$$

Notice that, one recovers the vertex used in Ref. [11] by setting $X_0^{[1]}(q) = 1$ in the above equations.

Substituting the form factors of $\bar{\Gamma}_{\text{BC}}^\mu(p_1, p_2, p_3)$ into Eqs. (3.11) and (3.12), we arrive at

the following coupled system for $A(p^2)$ and $B(p^2)$

$$A(p^2) = 1 + C_r g^2 Z_c^{-1} \int_k \frac{\mathcal{K}_0(p-k)}{A^2(k^2)k^2 + B^2(k^2)} \mathcal{K}_A^{\text{BC}}(k, p), \quad (3.23)$$

$$B(p^2) = C_r g^2 Z_c^{-1} \int_k \frac{\mathcal{K}_0(p-k)}{A^2(k^2)k^2 + B^2(k^2)} \mathcal{K}_B^{\text{BC}}(k, p), \quad (3.24)$$

where the kernel $\mathcal{K}_0(q)$ corresponds to the part that is not altered by the tensorial structure of the quark-gluon vertex, namely

$$\mathcal{K}_0(q) = \Delta(q)F(q)X_0^{[1]}(q), \quad (3.25)$$

while the parts that are affected, $\mathcal{K}_A^{\text{BC}}(k, p)$ and $\mathcal{K}_B^{\text{BC}}(k, p)$, are given by [8]

$$\begin{aligned} \mathcal{K}_A^{\text{BC}}(k, p) &= \frac{A(k^2)}{2p^2} [A(k^2) + A(p^2)] [3p \cdot k - 2h(p, k)] - 2B(k^2) \Delta B(k^2, p^2) \frac{h(p, k)}{p^2} \\ &\quad - A(k^2) \Delta A(k^2, p^2) \left[k^2 - \frac{(k \cdot p)^2}{p^2} + 2 \frac{k \cdot p}{p^2} h(p, k) \right], \end{aligned} \quad (3.26)$$

$$\mathcal{K}_B^{\text{BC}}(k, p) = \frac{3}{2} B(k^2) [A(k^2) + A(p^2)] + 2 [B(k^2) \Delta A(k^2, p^2) - A(k^2) \Delta B(k^2, p^2)] h(p, k),$$

where $h(p, k)$ is given by Eq. (3.10) and

$$\Delta A(k^2, p^2) \equiv \frac{A(k^2) - A(p^2)}{k^2 - p^2}, \quad \Delta B(k^2, p^2) \equiv \frac{B(k^2) - B(p^2)}{k^2 - p^2}. \quad (3.27)$$

Similarly, the effect of the vertex $\bar{\Gamma}_{\text{CP}}^\mu(p_1, p_2, p_3)$ is to replace the kernels $\mathcal{K}_A^{\text{BC}}(k, p)$ and $\mathcal{K}_B^{\text{BC}}(k, p)$ appearing in Eq. (3.23) and (3.24) by $\mathcal{K}_A^{\text{CP}}(k, p)$ and $\mathcal{K}_B^{\text{CP}}(k, p)$, respectively, where

$$\begin{aligned} \mathcal{K}_A^{\text{CP}}(k, p) &= \mathcal{K}_A^{\text{BC}}(k, p) + \frac{3k \cdot p}{2p^2} A(k^2) \Delta A(k^2, p^2) \frac{(k^2 - p^2)^2}{d(k, p)}, \\ \mathcal{K}_B^{\text{CP}}(k, p) &= \mathcal{K}_B^{\text{BC}}(k, p) + \frac{3}{2} B(k^2) \Delta A(k^2, p^2) \frac{(k^2 - p^2)^2}{d(k, p)}. \end{aligned} \quad (3.28)$$

Note that the above equations are written in the Euclidean space. Specifically, the Wick rotation was performed by setting $p^2 = -p_{\text{E}}^2$, $\Delta_{\text{E}}(p_{\text{E}}^2) = -\Delta(-p_{\text{E}}^2)$, $A(-p_{\text{E}}^2) = A_{\text{E}}(-p_{\text{E}}^2)$, and $B(-p_{\text{E}}^2) = B_{\text{E}}(-p_{\text{E}}^2)$. Therefore, $\Delta A(k^2, p^2)$, $\Delta B(k^2, p^2)$, and $h(p, k)$ change the sign under Wick rotation. For the integration measure, we used $\int_k = i \int_{k_{\text{E}}}$; as a last step, we have suppressed the subscript ‘‘E’’ everywhere.

D. Asymptotic behavior and renormalization group properties

The study of the ultraviolet (UV) behavior of the dynamical quark mass, $\mathcal{M}(p^2)$, predicted by the coupled system formed by Eqs. (3.23) and (3.24), reveals the need of one

final adjustment. Specifically, as is well known, the correct UV behavior for $\mathcal{M}(p^2)$ is given by [1, 2]

$$\mathcal{M}(x) = \frac{c}{x} \left[\ln \left(\frac{x}{\Lambda^2} \right) \right]^{\gamma_f - 1}, \quad (3.29)$$

where c is a μ -independent constant, related to the chiral condensate $\langle \bar{q}q \rangle_\mu$ by [8]

$$c = -\frac{4\pi^2\gamma_f}{3} \langle \bar{q}q \rangle_\mu \left[\ln \left(\frac{\mu^2}{\Lambda^2} \right) \right]^{-\gamma_f}. \quad (3.30)$$

and the mass anomalous dimension is given by $\gamma_f = 9C_r/(11C_A - 3/2C_r n_f)$. For the fundamental representation, we have $C_r = 4/3$ and then $\gamma_f = 12/(11C_A - 2n_f)$. Equivalently, we can rewrite it in terms of the first coefficient $b = (11C_A - 2n_f)/(48\pi^2)$ of the QCD β function, where $\gamma_f = 3C_F/(16\pi^2 b)$.

On the other hand, after setting $Z_1 = 1$ and $X_0^{[1]} = 1$, neglecting $\Delta A(k^2, p^2)$ and $\Delta B(k^2, p^2)$, and setting $A(p^2) = A(k^2) \rightarrow 1$, the asymptotic equation that the system (3.23)-(3.24) yields for $\mathcal{M}(p^2)$ is given, after the standard angular approximation, by

$$\mathcal{M}(p^2) = \frac{3C_r g^2}{16\pi^2} \left[\Delta(p^2)F(p^2) \int_0^{p^2} dk^2 \mathcal{M}(k^2) + \int_{p^2}^\infty dk^2 \Delta(k^2)F(k^2)\mathcal{M}(k^2) \right]. \quad (3.31)$$

In order to we verify whether indeed $\mathcal{M}(p^2)$ of Eq. (3.29) satisfies Eq. (3.31), we substitute $\mathcal{M}(p^2)$ into the rhs of Eq. (3.31), together with the one-loop gluon propagator

$$\Delta^{-1}(p^2) = p^2 \left[1 + \gamma_1 g^2 \ln \left(\frac{p^2}{\mu^2} \right) \right], \quad (3.32)$$

where $\gamma_1 = (\frac{13}{3}C_A - C_r n_f)/32\pi^2$, and the one-loop ghost dressing function

$$F^{-1}(p^2) = \left[1 + \frac{9}{4} \frac{C_A g^2}{48\pi^2} \ln \left(\frac{p^2}{\mu^2} \right) \right]. \quad (3.33)$$

After performing the above substitutions, it is straightforward to see that for asymptotic large values of p^2 , the dominant contribution comes from the first integral, and that the solution of Eq. (3.31) is indeed of the form given in (3.29), but with one important difference: the anomalous dimension assumes the value $\gamma_f = 36C_r/(35C_A - 6C_r n_f)$, instead of the correct value given above. Note that the difference is due to the non-Abelian contributions (gluons); setting $C_A = 0$, the two values coincide.

The reason for this discrepancy can be traced back to a typical ambiguity, intrinsic to the gauge-technique. Specifically, the standard procedure of constructing a vertex based

on the requirement that it should satisfy the correct STI, leaves the transverse (i.e. automatically conserved) part of the vertex undetermined [25, 28]. While, in the presence of mass gaps, the infrared dynamics appear to be largely unaffected, this ambiguity is known to modify the ultraviolet properties of the SD equations [25]. Essentially, failing to provide the correct transverse part leads to the mishandling of overlapping divergences, which, in turn, compromises the multiplicative renormalizability of the resulting SD equations. The construction of the appropriate transverse part is technically complicated even for QED [40], and its generalization to a non-abelian context is still pending. Given the expectation that the restoration of the transverse part should not affect the infrared dynamics, the usual short-cut employed in the literature is to account approximately for the missing pieces by modifying (by hand) the SDE in question.

Specifically, for the case at hand, the correct asymptotic behavior for $\mathcal{M}(p^2)$ may be restored by carrying out in Eqs. (3.23) and (3.24) the replacement

$$Z_c^{-1}\mathcal{K}_{A,B}(k,p) \rightarrow \mathcal{K}_{A,B}(k,p)F(p^2). \quad (3.34)$$

given that, for large p^2 , the perturbative (one-loop) expression for $F(p^2)$ is given by Eq.(3.33).

It is straightforward to verify that, with this modification, Eq. (3.31) yields the correct value for γ_f . Note that even though, strictly speaking, one needs to supply only the asymptotic form given in (3.33), it is natural to assume that the non-perturbative completion of this formula will be given by Eq. (4.3), namely the full $F(p^2)$.

At first sight it would seem that the modification introduced in Eq. (3.34) amounts to the counter-intuitive replacement $Z_c^{-1} \rightarrow F(p^2)$, i.e. trading a (cutoff-dependent) constant for a (μ -dependent) function of p^2 [11]. Even though from the operational point of view this is indeed what happens, the idea behind is slightly more subtle. A more intuitive way to interpret Eq. (3.34) is that the corresponding kernels are modified due to the presence of the (unknown) transverse parts, whose additional contributions must be such that, when properly renormalized, will effectively amount to the replacement given in Eq. (3.34). Needless to say, it would be very important to determine the precise mechanism that leads to these modifications, but this is at present beyond our powers.

It is instructive to understand from a slightly different (but ultimately equivalent) point of view why the (minimal) factor that must be supplied to Eq. (3.31) is indeed $F(p^2)$. The argument relies on the (expected) RG-invariance of the mass function $\mathcal{M}(p^2)$. Specifically,

let us for the moment assume that the underlying theory is QED, and set $F = 1$ into Eq. (3.31). Then, $\mathcal{M}(p^2)$ is RG-invariant, because, in QED, due to the abelian Ward identities, the product $g^2\Delta$ appearing on the rhs of Eq. (3.31) is RG-invariant. In the case of QCD this is no longer true in general; instead, in the R_ξ -type of gauges the corresponding RG-invariant combination is given by $g^2\Delta F^2$ [11, 41]. Therefore, the simplest way to convert the product $g^2\Delta F$ into a RG-invariant combination is to multiply it by F , which restores the RG-invariance of $\mathcal{M}(p^2)$.

IV. NUMERICAL ANALYSIS

In this section we will first review some of the recent lattice data for the gluon propagator $\Delta(q)$ and the ghost dressing function $F(q)$. Then, we will substitute them into Eq. (3.17), in order to obtain an estimate for $X_0^{[1]}(q)$. With all necessary ingredients [$\Delta(q)$, $F(q)$, and $X_0^{[1]}(q)$] available, we proceed to solve numerically the coupled system formed by the integral equations (3.23) and (3.24) when the non-abelian modifications of the BC and CP vertices are implemented. We will solve the corresponding equations both for fermions in the fundamental (quarks) and in the adjoint representations; for the former case we will use the numerical results obtained to compute the pion decay constant and the quark condensate.

A. Nonperturbative ingredients: gluon and ghost propagators from lattice and the form factor $X_0^{[1]}(q)$

In this subsection we will comment on the nonperturbative form of the three basic Green's functions entering into the gap equation, namely $\Delta(q)$, $F(q)$, and $X_0^{[1]}(q)$.

We start by showing on the left panel of Fig. 5 the lattice data for gluon propagator obtained in [18]. The lattice data presented there correspond to a $SU(3)$ quenched lattice simulation, where $\Delta(q)$ is renormalized at $\mu = 4.3$ GeV. In this plot, we clearly see the appearance of a plateau in the deep IR region. The IR finiteness of the gluon propagator has been long associated with the dynamical generation of an effective gluon mass [22, 32, 42]. In fact, the above set of lattice data can be accurately fitted in terms of the following physically

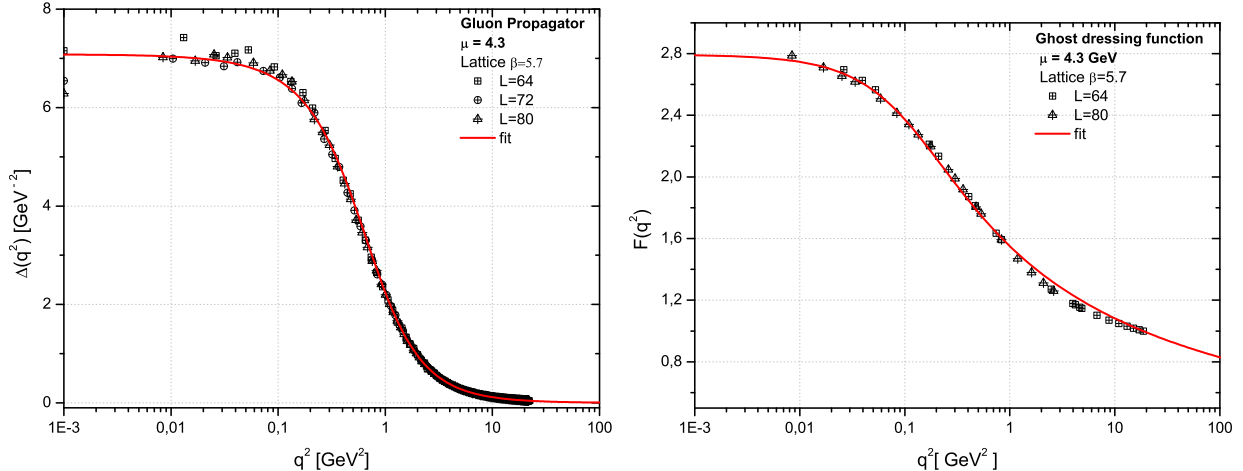


FIG. 5: Lattice results for the gluon propagator, $\Delta(q)$, and ghost dressing, $F(q)$, obtained in Ref. [18] and renormalized at $\mu = 4.3$ GeV. *Left panel:* The continuous line represents the gluon lattice data fitted by Eq. (4.1) when $m = 520$ MeV, $g_1^2 = 5.68$, $\rho_1 = 8.55$ and, $\rho_2 = 1.91$. *Right panel:* The lattice data for $F(q)$ fitted by Eq. (4.3) using $g_2^2 = 8.57$, $m = 520$ MeV, $\rho_3 = 0.25$ and, $\rho_4 = 0.68$.

motivated expression [43]

$$\Delta^{-1}(q^2) = m^2(q^2) + q^2 \left[1 + \frac{13C_A g_1^2}{96\pi^2} \ln \left(\frac{q^2 + \rho_1 m^2(q^2)}{\mu^2} \right) \right], \quad (4.1)$$

with $m^2(q^2)$ given by

$$m^2(q^2) = \frac{m^4}{q^2 + \rho_2 m^2}, \quad (4.2)$$

where the fitting parameters are $m = 520$ MeV, $g_1^2 = 5.68$, $\rho_1 = 8.55$ and, $\rho_2 = 1.91$. The parameter m acts as a physical mass scale, whose function is to regulate the perturbative RG logarithm; so, instead of diverging at the Landau pole, the logarithm saturates at a finite value [43]. In addition, for large values of q^2 , we recover the one-loop expression of the gluon propagator in the Landau gauge given by Eq. (3.32). Note that, contrary to conventional masses, dynamically generated masses display a non-trivial dependence on the momentum transfer q^2 [32]. In particular, $m^2(q^2)$ assumes a non-zero value in the IR, and drops rapidly in the UV in a way consistent with the operator product expansion [44–46].

On the right panel of Fig. 5, we show the lattice results for $F(q)$ obtained from [18]; evidently, $F(q)$ saturates in the deep IR at the constant value [22, 23]. The ghost dressing function is also renormalized at $\mu = 4.3$ GeV, and the data can be accurately fitted by the

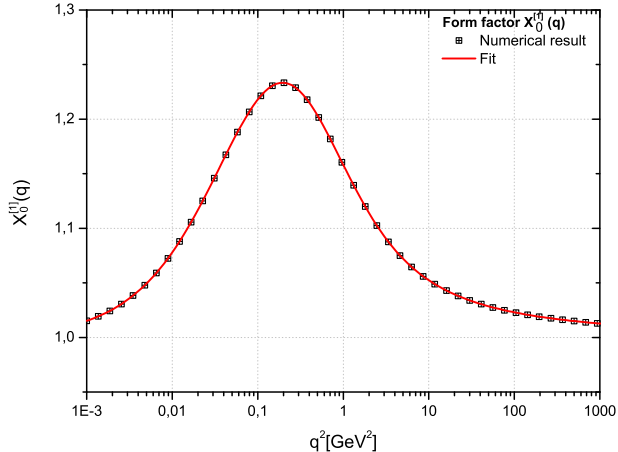


FIG. 6: Numerical result for the form factor $X_0^{[1]}(q)$ of the quark-ghost scattering kernel given by Eq. (3.17) when $\alpha(\mu^2) = 0.295$.

expression

$$F^{-1}(q^2) = 1 + \frac{9 C_A g_2^2}{4 48\pi^2} \ln \left(\frac{q^2 + \rho_3 m^2(q^2)}{\mu^2} \right), \quad (4.3)$$

where the dynamical mass is given by Eq. (4.2) changing the parameter $\rho_2 \rightarrow \rho_4$. The fitting parameters are $g_2^2 = 8.57$, $m = 520$ MeV, $\rho_3 = 0.25$ and, $\rho_4 = 0.68$.

The last ingredient to be determined is the form factor $X_0^{[1]}(q)$. We proceed substituting the fit for lattice data for $\Delta(q)$ and $F(q)$ presented in Fig. 5 into Eq. (3.17). Then, for determining the integral given by Eq. (3.17), we should fix the value of $g^2(\mu^2)$. We adopt the same procedure of Ref. [43], where it was found that the perturbative tail of effective coupling, determined from the lattice data, is compatible with four-loop perturbative calculation at MOM scheme, presented in [47]. More specifically, we use $\alpha(\mu^2) = g^2(\mu^2)/4\pi = 0.295$. The numerical result for $X_0^{[1]}(q)$ is shown in the Fig. 6, and it can be fitted by

$$a_2 + \frac{a_1 - a_2}{1 + (q^2/q_0^2)^p}, \quad (4.4)$$

where $a_1 = 1.0$, $a_2 = 1.27$, $q_0^2 = 0.027$ GeV² and, $p = 1.0$ when $q^2 \leq 0.202$ GeV²; while for $q^2 > 0.202$ GeV², we choose $a_1 = 1.40$, $a_2 = 1.0$, $q_0^2 = 0.45$ GeV² and, $p = 0.63$.

$X_0^{[1]}(q)$ shows a maximum located in the intermediate momentum region (around 450 MeV), while in the UV and IR regions $X_0^{[1]}(q) \rightarrow 1$. Although this peak is not very pronounced (notice the small scale in y-axis), we will see soon that it is essential for providing to the kernel of the gap equation the enhancement required for the generation of phenomenologically compatible constituent quark masses.

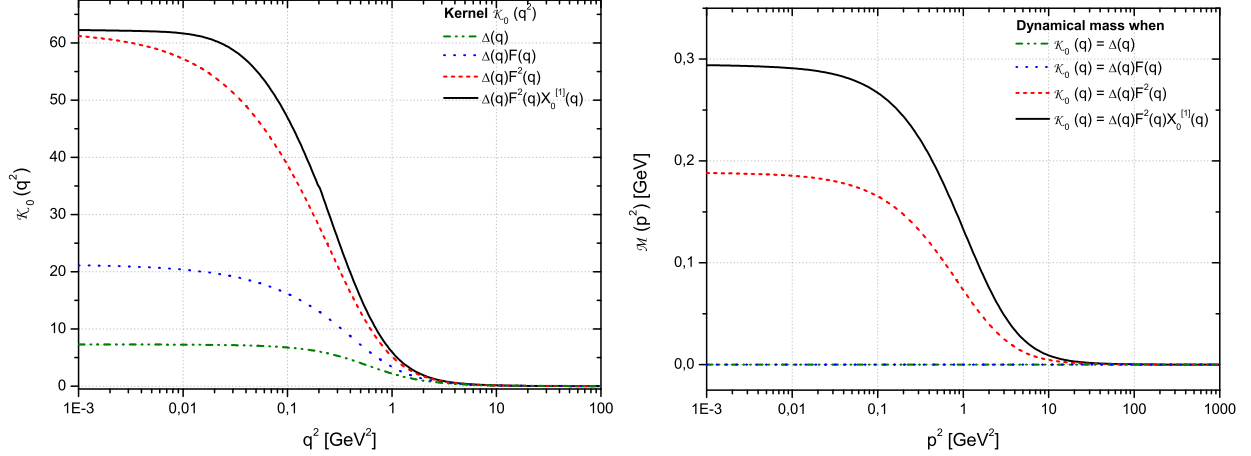


FIG. 7: *Left panel:* The individual contribution of the ingredients composing $\mathcal{K}_0(q)$. The green dotted-dashed line represents the case where $\mathcal{K}_0(q) = \Delta(q)$, the blue dotted line the case where $\mathcal{K}_0(q) = \Delta(q)F(q)$, in the red dashed curve $\mathcal{K}_0(q) = \Delta(q)F^2(q)$ and, finally the black continuous line represents the case where $\mathcal{K}_0(q)$ assumes the full form used in our calculation $\mathcal{K}_0(q) = \Delta(q)F^2(q)X_0^{[1]}(q)$. *Right panel:* The corresponding dynamical quark mass generated when we use in Eqs.(3.23) and (3.24) the different forms of $\mathcal{K}_0(q)$ are shown in the left panel.

B. Chiral symmetry breaking in the fundamental representation and the pion decay constant

We now proceed to the solution of the coupled system of integral equations defined by the Eqs.(3.23) and (3.24). Note that, in addition, and in accordance to the discussion given in subsection III D, we carry out the substitution

$$F(q) \rightarrow F^2(q), \quad (4.5)$$

in the Eq. (3.25). In other words, the kernel $\mathcal{K}_0(q)$ appearing on the rhs of Eqs.(3.25) and (3.24) will assume the final form

$$\mathcal{K}_0(q) = \Delta(q)F^2(q)X_0^{[1]}(q). \quad (4.6)$$

Before solving the system formed by Eqs.(3.23) and (3.24) with $\mathcal{K}_0(q)$ given by Eq. (4.6), it is instructive to study the numerical impact that each of the functions composing $\mathcal{K}_0(q)$ has on the value of the resulting quark mass.

The results of this exercise are presented in Fig. 7, where on the left panel we show the support that $\mathcal{K}_0(q)$ receives when we turn on one by one the Green's functions that

compose it. Without a doubt, the biggest numerical contribution comes from the ghost dressing function, $F(q^2)$. Nonetheless, one should not underestimate the effect caused by the scattering kernel, $X_0^{[1]}(q)$, which is responsible for a considerable contribution to the dynamical mass generation, as presented on the right panel of Fig. 7. On this panel, we show the corresponding dynamical quark masses that are obtained solving the system of Eqs.(3.25) and (3.24) when $\mathcal{K}_0(q)$ assumes one of the four forms presented in the left panel. Notice that, neither $\mathcal{K}_0(q) = \Delta(q)$ nor $\mathcal{K}_0(q) = \Delta(q)F(q)$ furnish the right amount of support necessary to trigger chiral symmetry breaking. The chiral symmetry is only broken when $\mathcal{K}_0(q) = \Delta(q)F^2(q)$ and, phenomenologically compatible values are only obtained when the effects of $X_0^{[1]}(q)$ are incorporated in the $\mathcal{K}_0(q)$. It is important to mention that, although $X_0^{[1]}(q)$ does not provide a sizable support for $\mathcal{K}_0(q)$ in the deep IR, the small contribution it furnishes in the intermediate region is enough for increasing the mass from $\mathcal{M}(0) = 190$ MeV to $\mathcal{M}(0) = 295$ MeV. This result is consistent with previous observations in the literature [9, 48], stating that the support crucial for quark generation originates from the intermediate region of the integration momenta.

Let us now return to the solution of the system formed by Eqs.(3.23) and (3.24). Substituting $\Delta(q^2)$, $F(q^2)$, and $X_0^{[1]}(q)$ into Eqs.(3.23) and (3.24), with the modification of Eq. (4.6), and fixing the Casimir eigenvalue in the fundamental representation *i.e.* $C_r = C_F = 4/3$, we determine numerically the unknown functions $A(p^2)$ and $B(p^2)$.

On the left panel of Fig. 8, the red dashed line represents the numerical result for the quark wave function $A^{-1}(p^2)$. As we can see, for large values of p^2 , the function $A(p^2)$ goes to 1, in agreement with the discussion presented in the Section III D. In the opposite limit, $A^{-1}(p^2)$ develops a plateau saturating in a finite value around 0.85.

The red dashed line in the right panel of Fig. 8 represents the corresponding dynamical quark mass $\mathcal{M}(p^2)$, obtained as the ratio $B(p^2)/A(p^2)$. One clearly sees that $\mathcal{M}(p^2)$ freezes out and acquires a finite value in the IR, while in the UV it shows the expected perturbative behavior given by Eq. (3.29) and represented by the blue dotted-dashed curve.

For the sake of comparison, we also solve numerically the coupled system when the non-abelian version of the CP vertex is employed. As we can see from the continuous black curve of Fig. 8, the qualitative behavior of the results obtained with the CP vertex is very similar to that obtained with the BC vertex. Note that both vertices generate phenomenologically acceptable values for $\mathcal{M}(0)$. More specifically, for the BC vertex we obtain $\mathcal{M}(0) = 294$ MeV

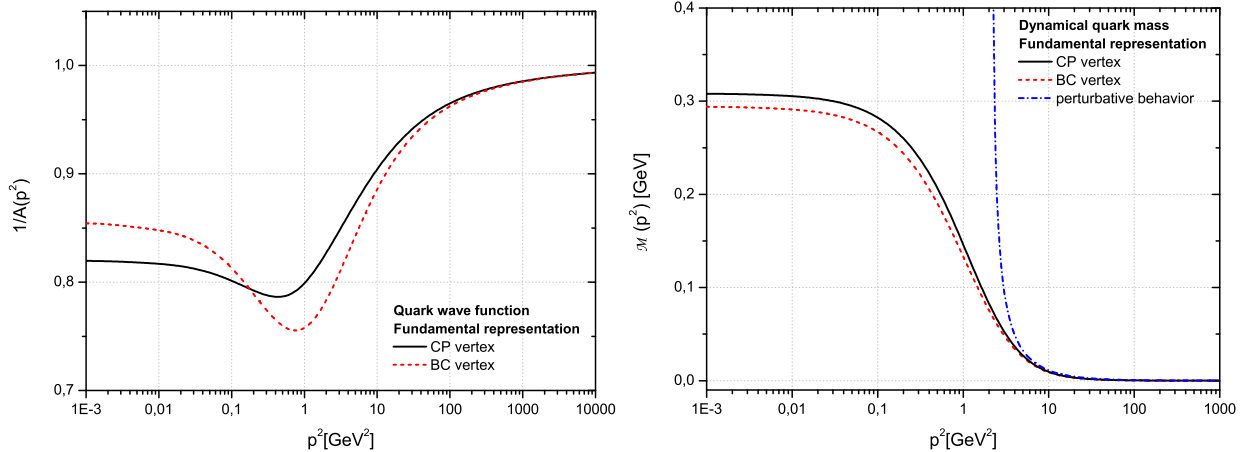


FIG. 8: *Left panel:* The numerical solution for the quark wave function $A^{-1}(p^2)$ in the fundamental representation when the non abelian versions of BC (red dashed curve) and CP (black continuous curve) vertices. are employed *Right panel:* The numerical solution for the dynamical quark mass $\mathcal{M}(p^2)$. The red dashed curve represents the dynamical mass generated when the BC vertex is used, while the black continuous line is the solution found with the CP vertex.

while for the CP vertex the value is slightly higher $\mathcal{M}(0) = 307$ MeV.

Once the behavior of the dynamical quark mass is determined, one may attempt to reproduce some of the phenomenological parameters that depend directly on it. Such a parameter is the pion decay constant f_π , which measures the “strength” of the CSB. The pion decay constant is defined through the axial-vector transition amplitude for an on-shell pion, $\langle 0 | A_5^{a\mu}(0) | \pi^b(k) \rangle = i f_\pi k^\mu \delta^{ab}$. Making use of the method developed by Pagels and Stokar [49], and Cornwall [50], \bar{f}_π can be expressed in terms of the dynamical quark mass as

$$\bar{f}_\pi^2 = \frac{3}{4\pi^2} \int_0^\infty dy \frac{\mathcal{M}(y)}{[y + \mathcal{M}^2(y)]^2} \left[\mathcal{M}(y) - \frac{y}{2} \frac{d\mathcal{M}(y)}{dy} \right]. \quad (4.7)$$

Substituting in the above equation the numerical solutions for $\mathcal{M}(p^2)$ presented in the Fig. 8, we obtain $\bar{f}_\pi = 64.3$ MeV for the case of the BC vertex, while with the CP vertex we get $\bar{f}_\pi = 68$ MeV. These values should be compared to the experimental value $f_\pi = 93$ MeV [51]. Evidently, the obtained values underestimate \bar{f}_π by almost 30%. The origin of this suppression could possibly be traced back to some of the approximation used for the quark-quark-pion proper vertex [50]. Some improved versions of Eq. (4.7) can be found in the literature; in particular, we will employ the expression of [52], where a correction term

is added to Eq. (4.7). More specifically,

$$f_\pi^2 = \bar{f}_\pi^2 + \delta f_\pi^2, \quad (4.8)$$

with

$$\delta f_\pi^2 = \frac{3}{4\pi^2} \int_0^\infty dy \left[y^3 \left(\frac{d\mathcal{M}(y)}{dy} \right)^2 - y^2 \mathcal{M}^2(y) \left(\frac{d\mathcal{M}^2(y)}{dy} \right) - y^2 \mathcal{M}^2(y) \frac{d\mathcal{M}(y)}{dy} \right]. \quad (4.9)$$

Adding this term to the expression of Eq. (4.7), we obtain $f_\pi = 76.4$ MeV for the case of the BC vertex, and $f_\pi = 80.6$ MeV for the CP vertex. Although the results are still below the experimental value, the correction added clearly contributes in the right direction.

Finally, we will compute the quark condensate, which plays the role of the order parameter for dynamical CSB. The quark condensate at scale of $\nu = 1 \text{ GeV}^2$ is given by [9]

$$\langle \bar{q}q \rangle (1 \text{ GeV}^2) = -\frac{3}{4\pi^2} \int_0^\nu dy \frac{y\mathcal{M}(y)}{A(y)[y + \mathcal{M}^2(y)]}. \quad (4.10)$$

Substituting again the solution $\mathcal{M}(p^2)$ and $A(p^2)$ presented in Fig. 8 into Eq. (4.10), we obtain $\langle \bar{q}q \rangle (1 \text{ GeV}^2) = (211 \text{ MeV})^3$ when the BC vertex is employed and $\langle \bar{q}q \rangle (1 \text{ GeV}^2) = (217 \text{ MeV})^3$. This value should be compared to the typical value of the quark condensate $\langle \bar{q}q \rangle (1 \text{ GeV}^2) = (229 \pm 9 \text{ MeV})^3$ [53].

C. Chiral symmetry breaking in the adjoint

Next we will solve the same system of integral equations formed by Eqs.(3.23) and (3.24) for both BC and CP kernels, given by Eqs. (3.27) and (3.28) respectively, when the Casimir eigenvalue in the adjoint representation *i.e.* $C_r = C_A = 3$.

When one switches from the fundamental to the adjoint representation, the overall effect in the gap equation is an enhancement factor of 9/4 due to the difference in the corresponding Casimir eigenvalues. Of course, due to the nonlinear nature of the gap equation, the wave function $A_{\text{adj}}^{-1}(p^2)$ and the adjoint mass $\mathcal{M}_{\text{adj}}(p^2)$ are not obtained from their quark counterparts through simple multiplication by 9/4.

The numerical results for the adjoint representation are shown in the Fig. 9. On the left panel, we compare the fermion wave functions, $A_{\text{adj}}^{-1}(p^2)$, when we use the modified BC and CP vertices. As expected, both solutions displays the right asymptotic behavior while in the IR limit the fermion wave functions saturate in smaller values compared to those of the

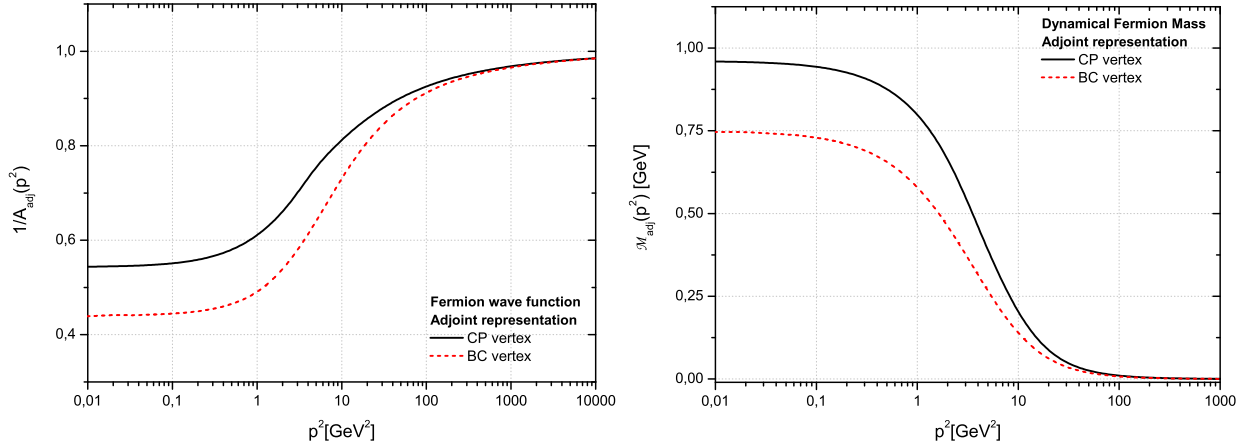


FIG. 9: *Left panel:* The numerical solution for the fermion wave function $A_{\text{adj}}^{-1}(p^2)$ in the adjoint representation when the modified BC vertex (dotted red curve) and the modified CP vertex (black continuous curve) are employed. *Right panel:* The numerical solution for the dynamical fermion mass $\mathcal{M}_{\text{adj}}(p^2)$. The dotted red curve represents the dynamical mass generated when the BC vertex is used. The black continuous line is the solution obtained with the CP vertex.

fundamental representation. In addition, we can notice that in the adjoint, $A_{\text{adj}}^{-1}(p^2)$ does not display anymore a minimum as it does in the fundamental representation.

On the right panel, we show the fermion dynamical mass $\mathcal{M}_{\text{adj}}(p^2)$. We see that the infrared saturation of $\mathcal{M}_{\text{adj}}(p^2)$ occurs for higher values compared to the values of $\mathcal{M}(p^2)$ in the fundamental. In particular, when the modified BC vertex is employed, one obtains $\mathcal{M}_{\text{adj}}(0) = 750$ MeV, while for the CP vertex $\mathcal{M}_{\text{adj}}(0) = 962$ MeV. Clearly we can see that the latter values are higher than $9/4\mathcal{M}(0)$. In addition, it is interesting to notice that the adjoint representation is more sensitive to the change from the BC to the CP vertex, since the difference between the results obtained with the both vertices is much more pronounced here than in the fundamental representation.

V. DISCUSSION AND CONCLUSIONS

In this article we have studied the CSB pattern that emerges when the gap equation is combined with the available lattice data for the gluon and ghost propagators [18]. Particular attention has been paid to the way the ghost sector enters into the gap equation. In particular, a complete Ansatz for the longitudinal part of the quark-gluon vertex has been constructed, which, in addition to the ghost-dressing function [11], captures the full depen-

dence on the various form factors composing the quark-ghost scattering kernel. This new vertex has been used to derive a more complete version of the gap equation, containing additional contributions from the quark-ghost scattering kernel. This latter quantity satisfies its own dynamical equation, which is coupled to the gap equation in a complicated way.

In order to reduce the complexity of the problem, we have restricted ourselves to the interplay of the gap equation with the only the scalar part, X_0 , of the quark-ghost scattering kernel, deriving its “one-loop dressed” expression. The form factor X_0 was then determined from this latter expression, for a special momentum configuration, using the lattice data for the gluon and ghost propagators appearing in it. The resulting expression for X_0 , shown in Fig. 6, reaches its maximum at a momentum of a few hundred MeV, where it displays a 25% enhancement compared to its tree-level value. We emphasize that the numerical effect of including X_0 into the gap equation is rather sizable; indeed, as can be seen from Fig. 7, it accounts for about 30% of the final result for the quark mass.

Finally, all ingredients are substituted into the gap equation, which is solved for the case of quarks (fundamental representation), and for fermions in the adjoint representation. The quark mass obtained is about 300 MeV, in good agreement with phenomenology, and is rather insensitive to the details of the quark-gluon vertex employed (BC vs CP). The corresponding mass obtained for the adjoint fermions displays a stronger dependence on the form of this vertex, varying between (750-962) MeV.

It is important to emphasize that there is a crucial complementarity between using lattice data as input into the gap equation, and, at the same time, employing an Ansatz for the vertex that captures suitably the dependence on quantities such as the ghost-dressing function and the quark-ghost scattering kernel. Indeed, the additional dependence on the ghost sector stemming from the vertex would be insufficient for getting the correct CSB if one were not to use the lattice results, which capture fully the underlying dynamics, displaying a sizable enhancement with respect to other non-perturbative approaches. Similarly, no realistic CSB pattern can be obtained if one were to substitute the lattice ingredients into the gap equation obtained from a less elaborate quark-gluon vertex, i.e., one that fails to include the effects due to the quark-ghost scattering kernel. Thus, at least within our framework, it is the interplay between these two points that finally provides an adequate description of CSB.

Amplifying on the previous point, let us mention that the SDE analysis presented in [22],

even though it reproduces qualitatively the lattice results, and most importantly accounts for the observed IR finiteness of the gluon propagator and the ghost-dressing function, it underestimates the size of both quantities by a significant amount. Clearly, it is an important challenge for the SDE approach of the PT-BFM formalism [22, 42, 54] to eliminate the aforementioned quantitative discrepancy. Perhaps the most obvious step would be to extend the analysis of [22] beyond the “one-loop dressed” approximation, given that there is no a-priori guarantee that the omitted “two-loop dressed” contributions are numerically depreciable. Needless to say, from the technical point of view, such an attempt would constitute a formidable task.

Another possible source of enhancement for the Green’s functions in question may be related to the non-trivial structure of the vacuum, and in particular with the presence of solitonic structures, such as vortices or monopoles. These classic field configurations are closely linked to the mechanisms of confinement [56] and CSB [57], and are known to affect the shape and size of the fundamental Green’s functions of the theory [58]. A particularly instructive example of how to include such effects at the level of the SDEs has been presented in [59].

Appendix A: The gap equation in the PT-BFM language

Given the recent reformulation of the SD series within the PT-BFM framework [42, 54, 60], it is conceptually interesting to re-express the gap equation using the PT-BFM terminology. Let us stress from the beginning, however, that, unlike what happens in the case of the gluon self-energy [54], where the corresponding SD equation in the PT-BFM formalism is vastly different from the conventional one, the gap equations obtained within both formalisms are completely identical.

Let us start the discussion by pointing out that the PT quark-self energy coincides with the conventional one in the Feynman gauge, both perturbatively (to all orders), as well as nonperturbatively. The reason has been explained in detail in the related literature; here it should suffice to mention that in the Feynman gauge there are no pinching momenta, and all three-gluon vertices appearing in the quark-self energy are “internal”, in the sense that all legs are irrigated by virtual momenta, and, therefore, they should not undergo the standard PT decomposition, a key ingredient in the construction of the PT gluon self-energy. An

equivalent way of saying this in the BFM language [35] is that, unlike gauge fields, fermionic fields are not split into a background and a quantum component. Therefore, the BFM fermion propagators are the same as the conventional ones (in all gauges). However, given that all nonperturbative ingredients we will use come from lattice simulations in the Landau gauge, the gap equation we study here is *not* the genuine PT gap equation. Away from the Feynman gauge, one must switch to the BFM language, or, equivalently, to the generalized PT. In any case, the central result remains the same: the gap equation in the Landau gauge is the same as the conventional one.

The PT-BFM gluon self-energy, denoted by $\widehat{\Delta}$, behaves in many aspects as that of QED; in particular, the product $g^2\widehat{\Delta}$ is RG-invariant (for any choice of the BFM gauge-fixing parameter). Of course, the propagator appearing in Eq. (2.15) is *not* $\widehat{\Delta}$ but rather the conventional Δ ; indeed, background field propagators do not propagate inside loops, only quantum ones. However, there exists a set of powerful identities that allows one to establish some important connections [41, 61, 62]. Specifically,

$$\begin{aligned}\Delta(q^2) &= [1 + G(q^2)]^2 \widehat{\Delta}(q^2), \\ F^{-1}(q^2) &= 1 + G(q^2) + L(q^2).\end{aligned}\tag{A1}$$

The functions $G(q^2)$ and $L(q^2)$ are the two form factors of a particular two-point function, denoted by $\Lambda_{\mu\nu}(q)$, defined as [54, 55]

$$\begin{aligned}\Lambda_{\mu\nu}(q) &= -ig^2 C_A \int_k H_{\mu\rho}^{(0)} D(k+q) \Delta^{\rho\sigma}(k) H_{\sigma\nu}(k, q) \\ &= g_{\mu\nu} G(q^2) + \frac{q_\mu q_\nu}{q^2} L(q^2).\end{aligned}\tag{A2}$$

Turns out that the function $L(q^2)$ is subleading both in the IR and in the UV; therefore, for the purposes of this argument can be safely neglected [41]. Then, the combination of the two identities in (A1) leads to the approximate relation

$$\widehat{\Delta}(q^2) = \Delta(q^2) F^2(q^2),\tag{A3}$$

leading to exactly the same conclusion as before.

Finally, the above discussion may be recast in the more intuitive language of an effective (running charge), traditionally employed in QED-inspired studies of QCD. From the (dimensionful) RG-invariant quantity $g^2\widehat{\Delta}$ introduced above, one may define a nonpertur-

bative effective charge, denoted by $\alpha(q^2)$, as

$$g^2 \widehat{\Delta}(q^2) = \frac{4\pi\alpha(q^2)}{q^2 + m^2(q^2)}, \quad (\text{A4})$$

where $m^2(q^2)$ is the momentum-dependent dynamical gluon mass, whose value in the deep IR is about (500 – 700) MeV. Using Eq. (A3), and after implementing Eq. (3.34), the alternative (and completely equivalent) form of Eq. (3.23) reads [6, 7] (setting $q \equiv p - k$)

$$A(p^2) = 1 + 4\pi C_r \int_k \frac{\alpha(q^2)}{q^2 + m^2(q^2)} \frac{\mathcal{K}_A(k, p)}{A^2(k^2)k^2 + B^2(k^2)}, \quad (\text{A5})$$

with an exactly analogous expression for $B(p^2)$. Note that finally there is no explicit reference to $F(q^2)$, because it has all been absorbed into the definition of the effective charge $\alpha(q^2)$. The RG-invariance of this equation can be easily established, given that both $\alpha(q^2)$, the gluon mass $m^2(q^2)$, are RG-invariant. The final inclusion of the $X_0^{[1]}$ into Eq. (A5) is straightforward.

Acknowledgments

The research of J. P. is supported by the European FEDER and Spanish MICINN under grant FPA2008-02878, and the Fundación General of the UV. The work of A.C.A is supported by the Brazilian Funding Agency CNPq under the grant 305850/2009-1.

-
- [1] H. D. Politzer, Nucl. Phys. B **117**, 397 (1976); H. D. Politzer, Phys. Lett. B **116**, 171 (1982).
- [2] V. A. Miransky and P. I. Fomin, Phys. Lett. B **105** (1981) 387; V. A. Miransky, Phys. Lett. B **165** (1985) 401.
- [3] D. Atkinson and P. W. Johnson, Phys. Rev. D **37**, 2296 (1988); Phys. Rev. D **37**, 2290 (1988); D. Atkinson, P. W. Johnson and K. Stam, Phys. Rev. D **37**, 2996 (1988).
- [4] N. Brown and M. R. Pennington, Phys. Rev. D **38**, 2266 (1988).
- [5] A. G. Williams, G. Krein and C. D. Roberts, Annals Phys. **210**, 464 (1991).
- [6] J. Papavassiliou and J. M. Cornwall, Phys. Rev. D **44**, 1285 (1991).
- [7] B. Haeri and M. B. Haeri, Phys. Rev. D **43**, 3732 (1991).
- [8] F. T. Hawes, C. D. Roberts and A. G. Williams, Phys. Rev. D **49**, 4683 (1994).
- [9] C. D. Roberts and A. G. Williams, Prog. Part. Nucl. Phys. **33**, 477 (1994).
- [10] A. A. Natale and P. S. Rodrigues da Silva, Phys. Lett. B **392**, 444 (1997).
- [11] C. S. Fischer and R. Alkofer, Phys. Rev. D **67**, 094020 (2003).
- [12] A. C. Aguilar, A. V. Nesterenko and J. Papavassiliou, J. Phys. G **31**, 997 (2005).
- [13] P. O. Bowman, U. M. Heller, D. B. Leinweber, M. B. Parappilly, A. G. Williams and J. b. Zhang, Phys. Rev. D **71**, 054507 (2005); W. Kamleh, P. O. Bowman, D. B. Leinweber, A. G. Williams and J. Zhang, Phys. Rev. D **76**, 094501 (2007).
- [14] V. Sauli, J. Adam and P. Bicudo, Phys. Rev. D **75**, 087701 (2007).
- [15] J. M. Cornwall, arXiv:0812.0359 [hep-ph].
- [16] A. Cucchieri and T. Mendes, PoS **LAT2007**, 297 (2007).
- [17] A. Cucchieri and T. Mendes, Phys. Rev. D **81**, 016005 (2010).
- [18] I. L. Bogolubsky, E. M. Ilgenfritz, M. Muller-Preussker and A. Sternbeck, PoS **LAT2007**, 290 (2007).
- [19] I. L. Bogolubsky, E. M. Ilgenfritz, M. Muller-Preussker and A. Sternbeck, Phys. Lett. B **676**, 69 (2009).
- [20] O. Oliveira and P. J. Silva, PoS **QCD-TNT09**, 033 (2009); arXiv:0910.2897 [hep-lat].
- [21] P. O. Bowman *et al.*, Phys. Rev. D **76**, 094505 (2007).
- [22] A. C. Aguilar, D. Binosi and J. Papavassiliou, Phys. Rev. D **78**, 025010 (2008).
- [23] Ph. Boucaud, J. P. Leroy, A. L. Yaouanc, J. Micheli, O. Pene and J. Rodriguez-Quintero,

- JHEP **0806** (2008) 012.
- [24] D. Dudal, S. P. Sorella, N. Vandersickel and H. Verschelde, Phys. Rev. D **77**, 071501 (2008).
 - [25] A. Salam, Phys. Rev. **130**, 1287 (1963); A. Salam and R. Delbourgo, Phys. Rev. **135**, B1398 (1964); R. Delbourgo and P. C. West, J. Phys. A **10**, 1049 (1977); R. Delbourgo and P. C. West, Phys. Lett. B **72**, 96 (1977).
 - [26] W. J. Marciano and H. Pagels, Phys. Rept. **36**, 137 (1978).
 - [27] A. I. Davydychev, P. Osland and L. Saks, Phys. Rev. D **63**, 014022 (2001).
 - [28] A. Kizilersu and M. R. Pennington, Phys. Rev. D **79**, 125020 (2009); A. Bashir, A. Kizilersu and M. R. Pennington, Phys. Rev. D **57**, 1242 (1998).
 - [29] F. Karsch and M. Lutgemeier, Nucl. Phys. B **550**, 449 (1999); Nucl. Phys. Proc. Suppl. **73**, 444 (1999).
 - [30] F. Basile, A. Pelissetto and E. Vicari, PoS **LAT2005**, 199 (2006); JHEP **0502**, 044 (2005).
 - [31] J. Engels, S. Holtmann and T. Schulze, PoS **LAT2005**, 148 (2006).
 - [32] J. M. Cornwall, Phys. Rev. D **26**, 1453 (1982).
 - [33] J. M. Cornwall and J. Papavassiliou, Phys. Rev. D **40**, 3474 (1989).
 - [34] D. Binosi and J. Papavassiliou, Phys. Rev. D **66**, 111901 (2002); J. Phys. G **30**, 203 (2004); A. Pilaftsis, Nucl. Phys. B **487**, 467 (1997).
 - [35] L. F. Abbott, Nucl. Phys. B **185**, 189 (1981).
 - [36] C. Itzykson and J-B. Zuber, *Quantum Field Theory* (McGraw-Hill, New York, 1980).
 - [37] J. C. Taylor, Nucl. Phys. B **33**, 436 (1971).
 - [38] J. S. Ball and T. W. Chiu, Phys. Rev. D **22**, 2542 (1980).
 - [39] G. Krein, P. Tang and A. G. Williams, Phys. Lett. B **215**, 145 (1988).
 - [40] D. C. Curtis and M. R. Pennington, Phys. Rev. D **42**, 4165 (1990).
 - [41] A. C. Aguilar, D. Binosi, J. Papavassiliou and J. Rodriguez-Quintero, Phys. Rev. D **80**, 085018 (2009).
 - [42] A. C. Aguilar and J. Papavassiliou, JHEP **0612**, 012 (2006).
 - [43] A. C. Aguilar, D. Binosi and J. Papavassiliou, JHEP **1007**, 002 (2010).
 - [44] A. C. Aguilar and J. Papavassiliou, Eur. Phys. J. A **35**, 189 (2008).
 - [45] M. Lavelle, Phys. Rev. D **44**, 26 (1991).
 - [46] D. Dudal, J. A. Gracey, S. P. Sorella, N. Vandersickel and H. Verschelde, Phys. Rev. D **78**, 065047 (2008).

- [47] Ph. Boucaud *et al.*, Phys. Rev. D **74**, 034505 (2006); Ph. Boucaud, F. De Soto, J. P. Leroy, A. Le Yaouanc, J. Micheli, O. Pene and J. Rodriguez-Quintero, Phys. Rev. D **79**, 014508 (2009).
- [48] P. Maris and P. C. Tandy, Phys. Rev. C **60**, 055214 (1999).
- [49] H. Pagels and S. Stokar, Phys. Rev. D **20**, 2947 (1979).
- [50] J. M. Cornwall, Phys. Rev. D **22**, 1452 (1980).
- [51] K. Nakamura [Particle Data Group], J. Phys. G **37**, 075021 (2010).
- [52] A. Barducci, R. Casalbuoni, M. Modugno, G. Pettini and R. Gatto, Phys. Lett. B **405**, 173 (1997).
- [53] J. Gasser and H. Leutwyler, Phys. Rept. **87**, 77 (1982); L. J. Reinders, H. Rubinstein and S. Yazaki, Phys. Rept. **127**, 1 (1985); H. G. Dosch and S. Narison, Phys. Lett. B **417**, 173 (1998); C. McNeile, Phys. Lett. B **619**, 124 (2005); V. Gimenez, V. Lubicz, F. Mescia, V. Porretti and J. Reyes, Eur. Phys. J. C **41**, 535 (2005).
- [54] D. Binosi and J. Papavassiliou, Phys. Rept. **479**, 1 (2009).
- [55] A. C. Aguilar, D. Binosi and J. Papavassiliou, JHEP **0911**, 066 (2009).
- [56] J. Greensite and S. Olejnik, Phys. Rev. D **67**, 094503 (2003).
- [57] P. de Forcrand and M. D'Elia, Phys. Rev. Lett. **82**, 4582 (1999).
- [58] J. Gattnar, K. Langfeld and H. Reinhardt, Phys. Rev. Lett. **93**, 061601 (2004).
- [59] A. P. Szczepaniak and H. H. Matevosyan, Phys. Rev. D **81**, 094007 (2010).
- [60] D. Binosi and J. Papavassiliou, JHEP **0811**, 063 (2008).
- [61] P. A. Grassi, T. Hurth and M. Steinhauser, Annals Phys. **288**, 197 (2001).
- [62] D. Binosi and J. Papavassiliou, Phys. Rev. D **66**, 025024 (2002).